

Perturbative Variational Quantum Eigensolver based on Reduced Density Matrix Method

Yuhan Zheng,^{†,ⓐ} Yibin Guo,^{‡,¶,§,ⓐ} Huili Zhang,[‡] Jie Liu,^{*,||} Xiongzhi Zeng,^{*,⊥}
Xiaoxia Cai,^{*,#} Zhenyu Li,^{*,⊥,||} and Jinlong Yang^{⊥,||}

[†]*State Key Laboratory of Precision and Intelligent Chemistry, University of Science and
Technology of China, Hefei, Anhui 230026, China*

[‡]*Beijing Academy of Quantum Information Sciences, Beijing, China*

[¶]*Institute of Physics, Chinese Academy of Sciences, Beijing 100190, China*

[§]*University of Chinese Academy of Sciences, Beijing 101408, China*

^{||}*Hefei National Laboratory, University of Science and Technology of China, Hefei 230088,
China*

[⊥]*State Key Laboratory of Precision and Intelligent Chemistry, University of Science and
Technology of China, Hefei, Anhui 230026, China*

[#]*Institute of High Energy Physics, Chinese Academy of Sciences, Beijing 100049, China*

[ⓐ]*These authors contributed equally.*

E-mail: liujie86@ustc.edu.cn; xzzeng@ustc.edu.cn; xxcai@ihep.ac.cn; zyli@ustc.edu.cn

Abstract

Current noisy intermediate-scale quantum (NISQ) devices lack the quantum resources required for practical applications. To address this, we propose the perturbative variational quantum eigensolver (PT-VQE). In PT-VQE, VQE is used to capture key correlations within a carefully selected active space, while perturbation theory efficiently incorporates interactions in the remaining space, without requiring additional

qubits or circuit depth. When the VQE-optimized state closely approximates the true ground state in the active space, excitations cannot act solely in the active space, since their contributions to perturbative correction are negligible. This reduces the highest-order required RDM from 4-RDM to 3-RDM, significantly reducing computational costs. We validate PT-VQE by calculating the ground-state potential energy surfaces (PESs) of HF and N₂, as well as the ground-state energy of ferrocene (Fe(C₅H₅)₂). Additionally, PT-VQE is performed on a quantum computer to compute the PES of F₂. The consistent results obtained from both PT-VQE with the highest 3-RDM and 4-RDM confirm the reliability of the constraint. PT-VQE significantly outperforms standard VQE, achieving chemical accuracy. This method offers a resource-efficient and practical approach for accurate quantum simulations of larger systems.

1 Introduction

Accurate determination of the electronic structure is at the core of computational chemistry, enabling prediction of molecular properties, reaction mechanisms, and material behaviors. Traditional methods such as density functional theory and coupled cluster have achieved remarkable success in scalability and accuracy for weakly correlated systems. An accurate description of strongly correlated chemical systems requires an adequate treatment of both static and dynamic electron correlation, which presents a great challenge for quantum chemistry.

Multireference methods, such as the complete active space self-consistent field (CASSCF) approach, are widely employed to capture static correlation effects.¹ To overcome the computational limitations of exact diagonalization, a diverse array of solvers has been developed, including selected configuration interaction (CI) methods,²⁻⁵ full CI quantum Monte Carlo,^{6,7} the density matrix renormalization group (DMRG),^{8,9} and many-body expanded full CI techniques.^{10,11} As the rapid advance in quantum information technology, quantum computing offers a promising alternative for exact diagonalization by leveraging the inher-

ent parallelism of quantum states to solve the electronic Schrödinger equation efficiently. Among quantum algorithms, the variational quantum eigensolver (VQE) has emerged as a leading candidate for near-term quantum devices, combining quantum state preparation with classical optimization to approximate ground-state energies. However, these methods are constrained by small active space, hindering their applications to large systems.

To bridge this gap, integrating perturbation theory—a cornerstone of classical quantum chemistry—with exact diagonalization methods presents a compelling strategy. Perturbation methods, such as Møller-Plesset (MP) theory, systematically correct approximate solutions (e.g., Hartree-Fock) by accounting for electron correlation effects through hierarchical expansions. The combination of perturbation theory (PT) and exact diagonalization methods, such as complete active space second-order perturbation theory (CASPT2)¹² and N-electron valence second-order perturbation theory (NEVPT2),¹³ has been widely used. Similarly, by hybridizing VQE with perturbation theory, one can delegate the computationally demanding high-precision corrections to classical post-processing, thereby reducing the quantum resource overhead. This synergy capitalizes on the quantum computer’s ability to efficiently generate a low-rank approximation of the wavefunction, while classical perturbation theory refines the result to chemical accuracy. Such an approach not only mitigates the impact of quantum hardware limitations but also aligns with the hybrid quantum-classical paradigm central to noisy intermediate-scale quantum (NISQ)-era algorithms.

Recent advances in quantum simulation have highlighted the growing interest in integrating perturbation theory to accurately and efficiently capture electron correlation effects. Ryabinkin et al. established an a posteriori PT correction derived from an effective Hamiltonian in the qubit representation, further advancing the development of VQE-PT algorithms for molecular excited-state simulations.¹⁴ Concurrently, Liu et al. proposed perturbative variational quantum algorithms for material simulations, in which the perturbative wave function was represented as a linear combination of excited states generated by applying an anti-Hermitian excitation operator to a multireference wave function.¹⁵ These two methods

suggest recovering the accurate correlation energy by applying PT correction to a shallow-circuit VQE calculation based on the active space approach. To extend beyond active space, Tammaro et al. introduced a VQE-based formulation of N-electron valence PT, in which the perturbation correction is computed using excited states obtained from quantum subspace expansion (QSE). This method is used to investigate the relative stability of the hydroxide anion and hydroxyl radical, demonstrating its potential for molecular systems.¹⁶ Liepuoniute et al. simulated a Diels-Alder reaction on a quantum computer by combining CASPT2, in which the CI coefficients were extracted from a quantum state, the QSE calculation was performed to approximate the ground-state wave function, and the reduced density matrices were computed in an active space.¹⁷ These methods were formulated based on the Dyall Hamiltonian and the perturbation correction was computed with the help of QSE.

In this work, we integrate VQE with PT, offering a promising strategy to leverage the strengths of both approaches. In this method, the VQE is used to generate a multireference wave function, which captures strong electron correlations within the active space, while PT is used to recover the remaining electron correlation. Perturbation energies are computed using reduced density matrices (RDMs) measured on the quantum computer, without additional increase in qubits or circuit depth. Measuring RDMs is significantly simpler than reconstructing the entire wavefunction, yet most system properties of interest can be derived from RDMs.¹⁸ In order to mitigate the effect of noise on RDMs, we optimize the RDMs with N-representability conditions to enhance their accuracy. We apply this method to study the PES of the fluorine molecule, achieving a high accuracy quantum simulation of electronic structure.

2 Theory

In many quantum chemistry calculations, the complexity of the system requires efficient allocation of computational resources. To address this, molecular orbital space is typically

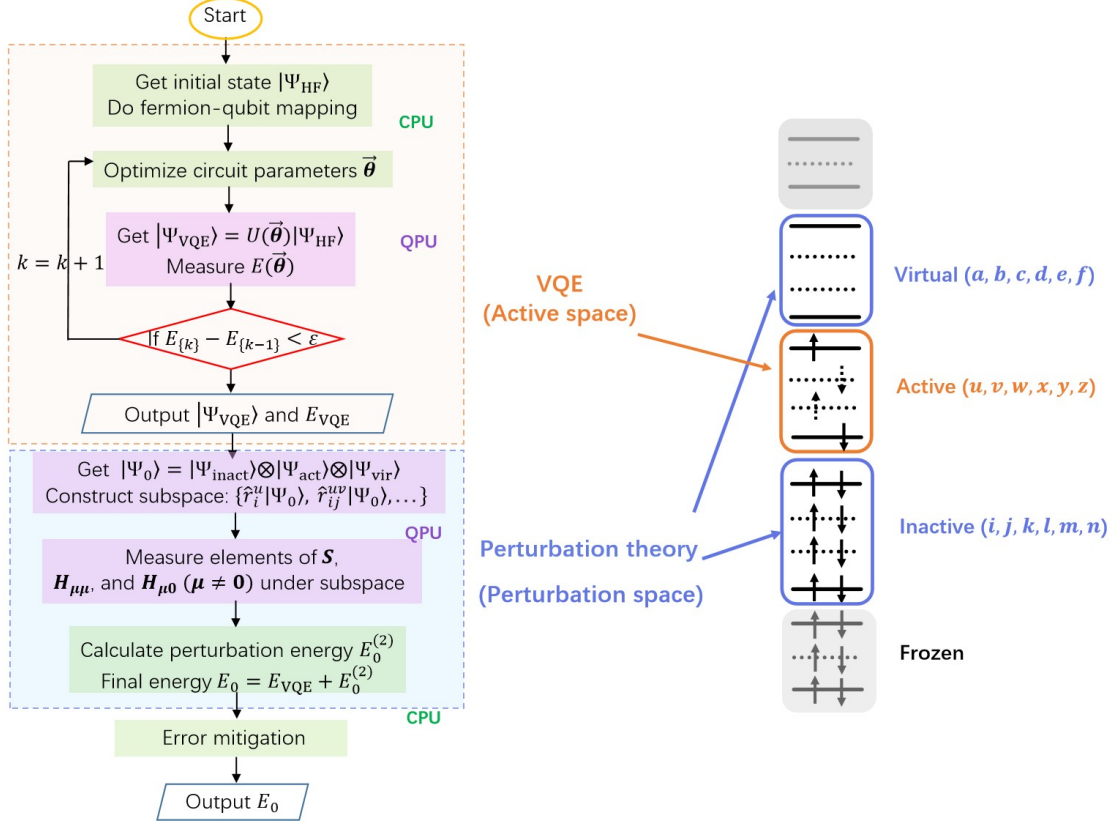


Figure 1 Algorithm flow chart and spatial partitioning

divided into distinct regions based on their relevance to the problem under consideration. As illustrated in Fig. 1, the total orbital space is partitioned into three regions: active, perturbative, and frozen. The perturbative space is further divided into the fully occupied inactive space and the unoccupied virtual space. A variational quantum algorithm is applied within the active space, which contains the most essential orbitals, to compute a reference ground state. The perturbative space is then incorporated to capture additional interactions, improving the accuracy of ground-state calculations.

Using variational quantum algorithms, the ground state within active space is expressed as a product of unitary transformations generated by single and double excitation operators:

$$|\Psi_{\text{act}}(\boldsymbol{\theta})\rangle = U(\boldsymbol{\theta})|\Psi_{\text{HF}}\rangle = \prod_{k=1}^N e^{\theta_k \hat{\tau}_k} |\Psi_{\text{HF}}\rangle \quad (1)$$

where $\boldsymbol{\theta} = \{\theta_1, \theta_2, \dots, \theta_N\}$ is a set of variational parameters, and each $\hat{\tau}_\mu$ is an anti-

Hermitian operator defined as

$$\hat{\tau}_\mu = \hat{T}_\mu - \hat{T}_\mu^\dagger, \quad (2)$$

where \hat{T}_μ represents all possible single and double excitation operators within the active space: $\hat{T}_\mu \in \{\hat{a}_u^\dagger \hat{a}_v, \hat{a}_u^\dagger \hat{a}_v^\dagger \hat{a}_w \hat{a}_x\}$ with u, v, w, x, \dots denoting spin orbitals in active space. Spin orbitals in the inactive space are denoted by i, j, k, \dots , while those in the virtual space are denoted by a, b, c, \dots . In this work, the Hartree-Fock state within the active space is used as the initial state, and the wave function $|\Psi_{\text{act}}(\boldsymbol{\theta})\rangle$ is obtained using the adaptive derivative-assembled pseudo-Trotter (ADAPT) VQE¹⁹ method with the approximate ground-state energy E_{VQE} . The reference ground state is defined as:

$$|\Psi_0\rangle = |\Psi_{\text{inact}}\rangle \otimes |\Psi_{\text{act}}(\boldsymbol{\theta})\rangle \otimes |\Psi_{\text{vir}}\rangle \quad (3)$$

where $|\Psi_{\text{inact}}\rangle$ and $|\Psi_{\text{vir}}\rangle$ represent fully occupied and fully unoccupied (vacuum) states in inactive and virtual spaces, respectively.

To incorporate the effects of the perturbative space for a more accurate ground state and its energy, we use $|\Psi_0\rangle$ as a reference to construct a subspace that captures additional configurations. We introduce excitation operators $\hat{\tau}_\mu$ to excite electrons from the occupied orbitals of $|\Psi_0\rangle$ to unoccupied orbitals in either the active space or the virtual space.

$$\begin{aligned} \hat{E}_q^p &= a_p^\dagger a_q + a_{\bar{p}}^\dagger a_{\bar{q}} \\ \hat{E}_{rs}^{pq} &= \hat{E}_r^p \hat{E}_s^q + \hat{E}_s^p \hat{E}_r^q = 2a_p^\dagger a_q^\dagger a_r a_s + 2a_{\bar{p}}^\dagger a_{\bar{q}}^\dagger a_{\bar{r}} a_{\bar{s}} + a_p^\dagger a_q^\dagger a_{\bar{r}} a_s \\ &\quad + a_p^\dagger a_q^\dagger a_r a_{\bar{s}} + a_{\bar{p}}^\dagger a_{\bar{q}}^\dagger a_r a_{\bar{s}} + a_{\bar{p}}^\dagger a_{\bar{q}}^\dagger a_{\bar{r}} a_s \quad (\text{type1}) \\ \hat{E}_{rs}^{pq} &= \hat{E}_r^p \hat{E}_s^q - \hat{E}_s^p \hat{E}_r^q = a_p^\dagger a_q^\dagger a_{\bar{r}} a_s + a_p^\dagger a_q^\dagger a_r a_{\bar{s}} + a_{\bar{p}}^\dagger a_{\bar{q}}^\dagger a_r a_{\bar{s}} + a_{\bar{p}}^\dagger a_{\bar{q}}^\dagger a_{\bar{r}} a_s \quad (\text{type2}) \end{aligned} \quad (4)$$

\hat{E}_q^p and \hat{E}_{pq}^{rs} here are spin-adapted operators,^{20,21} and the bar over a subscript indicates the spin orbital is spin-down. The excitation operators $\hat{\tau}_\mu = \hat{E}_\mu - \hat{E}_\mu^\dagger$ are anti-Hermitian to ensure that the basis vectors $\{|\bar{\Psi}_\mu\rangle = \hat{\tau}_\mu |\Psi_0\rangle\}$ are orthogonal to the reference ground state

$|\Psi_0\rangle$. In this work, a set of single and double excitations is taken into account $\{\hat{r}_\mu\} = \{\hat{r}_i^u, \hat{r}_i^a, \hat{r}_u^a, \hat{r}_{ij}^{uv}, \hat{r}_{ij}^{ab}, \hat{r}_{uv}^{ab}, \hat{r}_{wi}^{uv}, \hat{r}_{vi}^{au}, \hat{r}_{vw}^{au}, \hat{r}_{ij}^{au}, \hat{r}_{ui}^{ab}\}$. The basis vectors can be orthonormalized by the following formula:

$$|\Psi_\mu\rangle = \sum_{\alpha \neq 0} \mathbf{S}^{-\frac{1}{2}}{}_{\alpha\mu} |\bar{\Psi}_\alpha\rangle \quad (5)$$

where \mathbf{S} is the overlap matrix with $S_{\mu\nu} = \langle \bar{\Psi}_\mu | \bar{\Psi}_\nu \rangle$. Since $|\Psi_0\rangle$ is orthogonal to all $|\bar{\Psi}_\mu\rangle$, the index 0 is excluded from the summation. The optimized ground state is expressed as a linear combination of these $K + 1$ orthonormal basis vectors

$$|\Psi\rangle \approx \sum_{\mu=0}^K d_\mu |\Psi_\mu\rangle. \quad (6)$$

The matrix expression of the Schrödinger equation within this subspace is:

$$\mathbf{H}\mathbf{d} = E_0\mathbf{d}. \quad (7)$$

where E_0 is the ground-state energy after incorporating perturbative space, $H_{\mu\nu} = \langle \Psi_\mu | \hat{H} | \Psi_\nu \rangle$, and the μ th component of the column vector \mathbf{d} is d_μ .

Efficient approximation of ground-state energy E_0 via perturbation theory.

If the subspace (the number of excitation operators) becomes too large, the measurement of the full matrices \mathbf{H} and \mathbf{S} can be computationally expensive. In such cases, PT provides an efficient alternative for approximating E_0 , which reduces computational cost while maintaining accuracy.

$$\begin{aligned} \hat{H}^{(0)} &= \sum_{\mu=0}^K H_{\mu\mu} |\Psi_\mu\rangle \langle \Psi_\mu| \\ \hat{H}^{(1)} &= \hat{H} - \hat{H}^{(0)} = \sum_{\substack{\mu,v=0 \\ (\mu \neq v)}}^K H_{\mu\nu} |\Psi_\mu\rangle \langle \Psi_\nu| \end{aligned} \quad (8)$$

Thus, $\hat{H}^{(0)} |\Psi_\mu\rangle = E_\mu^{(0)} |\Psi_\mu\rangle$, i.e., $|\psi_\mu\rangle^{(0)} = |\Psi_\mu\rangle$ and $E_\mu^{(0)} = \langle \Psi_\mu | \hat{H} | \Psi_\mu \rangle$. Note that $E_0^{(0)} =$

E_{VQE} . According to perturbation theory,²² we have

$$\begin{aligned}
|\psi_0^{(1)}\rangle &= \sum_{\mu=1}^K \frac{\langle \psi_\mu^{(0)} | \hat{H}^{(1)} | \psi_0^{(0)} \rangle}{E_0^{(0)} - E_\mu^{(0)}} |\psi_\mu^{(0)}\rangle = \sum_{\mu=1}^K \frac{\langle \Psi_\mu | \hat{H} | \Psi_0 \rangle}{E_0^{(0)} - E_\mu^{(0)}} |\Psi_\mu\rangle \\
E_0^{(1)} &= \langle \psi_0^{(0)} | \hat{H}^{(1)} | \psi_0^{(0)} \rangle = 0 \\
E_0^{(2)} &= \langle \psi_0^{(0)} | \hat{H}^{(1)} | \psi_0^{(1)} \rangle = \sum_{\mu=1}^K \frac{|\langle \Psi_\mu | \hat{H} | \Psi_0 \rangle|^2}{E_0^{(0)} - E_\mu^{(0)}}
\end{aligned} \tag{9}$$

Finally, we get

$$E_0 = E_{\text{VQE}} + \sum_{\mu=1}^K \frac{|\langle \Psi_\mu | \hat{H} | \Psi_0 \rangle|^2}{E_0^{(0)} - E_\mu^{(0)}} \tag{10}$$

Given the form of $|\Psi_0\rangle$ as shown in Eq. (3), the inactive space is entirely frozen, leaving only the active space relevant for measurement. With this setup, $\langle \Psi_\mu | \hat{H} | \Psi_\nu \rangle = \langle \Psi_0 | \hat{r}_\mu^\dagger \hat{H} \hat{r}_\nu | \Psi_0 \rangle$ can be measured exclusively within the active-space VQE circuit. To illustrate this more clearly, the measured terms in $E_0^{(2)}$ are expressed as several k -particle reduced density matrices (k -RDMs), with general form:

$${}^k D_{q_1 q_2 \dots q_k}^{p_1 p_2 \dots p_k} = \frac{1}{k!} \langle \Psi_{\text{act}} | a_{p_1}^\dagger a_{p_2}^\dagger \dots a_{p_k}^\dagger a_{q_k} a_{q_{k-1}} \dots a_{q_1} | \Psi_{\text{act}} \rangle \tag{11}$$

The second-quantized Hamiltonian is given by:

$$\hat{H} = \sum_{pq} h_{pq} a_p^\dagger a_q + \frac{1}{2} \sum_{pqrs} h_{pqrs} a_p^\dagger a_q^\dagger a_r a_s + C \tag{12}$$

In the following, u, v, w, x, y, z, t, m represent active orbitals, while p, q, r, s denote general orbitals, including inactive, active, and virtual orbitals. The highest-order RDM required in PT-VQE is 4-RDM, related to 2-electron interaction term $V = \frac{1}{2} \sum_{pqrs} h_{pqrs} a_p^\dagger a_q^\dagger a_r a_s$, as

shown below:

$$\begin{aligned}
V_{wx}^{uv} &= \langle \Psi_0 | (a_u^\dagger a_v^\dagger a_w a_x - a_x^\dagger a_w^\dagger a_v a_u)^\dagger \frac{1}{2} \sum_{pqrs} h_{pqrs} (a_p^\dagger a_q^\dagger a_r a_s) | \Psi_0 \rangle \\
&= \sum_{yztm} h_{yztm} [(\delta_{uy}\delta_{vz} - \delta_{vy}\delta_{uz})^2 D_{mt}^{xw} - 3\delta_{uy}^3 D_{mtv}^{xwz} + 3\delta_{vy}^3 D_{mtu}^{xwz} + 3\delta_{uz}^3 D_{mtv}^{xwy} \\
&\quad - 3\delta_{zv}^3 D_{mtu}^{xwy} + 12^4 D_{mtuv}^{xwyz} - (\delta_{xy}\delta_{wz} - \delta_{wy}\delta_{xz})^2 D_{mt}^{uw} + 3\delta_{xy}^3 D_{mtw}^{uvw} - 3\delta_{wy}^3 D_{mtx}^{uvw} \\
&\quad - 3\delta_{xz}^3 D_{mtw}^{uvw} + 3\delta_{zw}^3 D_{mtx}^{uvw} - 12^4 D_{mtxw}^{uvw}]
\end{aligned} \tag{13}$$

If the state computed by the VQE method is a good approximation to the ground state in the active space, we can exclude excitations restricted to the active space, i.e., \hat{r}_v^u and \hat{r}_{wx}^{uv} , because their contributions to the ground-state energy correction approximate zero. After ignoring these excitations, all $\hat{E}_\mu |\Psi_0\rangle$ are already orthogonal to $|\Psi_0\rangle$. Thus, excitation operators \hat{r}_μ no longer need to be anti-Hermitian, i.e., they do not require the transformation $\hat{E}_\mu - \hat{E}_\mu^\dagger$, and we can simply take $\hat{r}_\mu = \hat{E}_\mu$. In this situation, the highest-order RDM required reduces to 3-RDM, shown in following terms:

$$\begin{aligned}
V_{wi}^{uv} &= \langle \Psi_0 | (a_u^\dagger a_v^\dagger a_w a_i)^\dagger \frac{1}{2} \sum_{pqrs} h_{pqrs} (a_p^\dagger a_q^\dagger a_r a_s) | \Psi_0 \rangle \\
&= \sum_{xyz} (h_{xyzi} - h_{xyiz}) \left[\frac{1}{2} (\delta_{ux}\delta_{vy} - \delta_{vx}\delta_{uy})^2 D_z^w - \delta_{ux}^2 D_{vz}^{wy} \right. \\
&\quad \left. + \delta_{vx}^2 D_{uz}^{wy} + \delta_{uy}^2 D_{vz}^{wx} - \delta_{vy}^2 D_{uz}^{wx} + 3^3 D_{vuz}^{wxy} \right]
\end{aligned} \tag{14}$$

$$\begin{aligned}
V_{vw}^{au} &= \langle \Psi_0 | (a_a^\dagger a_u^\dagger a_v a_w)^\dagger \frac{1}{2} \sum_{pqrs} h_{pqrs} (a_p^\dagger a_q^\dagger a_r a_s) | \Psi_0 \rangle \\
&= \sum_{xyz} (h_{axyz} - h_x a y z) (\delta_{ux}^2 D_{yz}^{vw} - 3^3 D_{uyz}^{vwx})
\end{aligned} \tag{15}$$

Following the operator selection method in Ref. 23, we can use the computed values of each term $W_\mu = \frac{|\langle \Psi_\mu | \hat{H} | \Psi_0 \rangle|^2}{E_0^{(0)} - E_\mu^{(0)}}$ in $E_0^{(2)}$ to further reduce the dimension of the basis set $\{|\Psi_\mu\rangle\}$. Since W_μ quantifies the contribution of the excitation operator \hat{r}_μ to the ground-state energy correction, it enables a prioritized selection of the most relevant excitations.

3 k -RDM measurement

Quantum state tomography reconstructs a quantum state by measuring it in a complete basis. However, the number of required measurement bases grows exponentially with the system size. To mitigate this, we introduce efficient methods for measuring k -RDM that reduce computational complexity.

Grouping utilizes the fact that mutually commuting observables share common eigenstates and can be measured simultaneously, reducing the number of measurements. Pauli strings can be grouped based on two types of commutation relations: qubit-wise commutativity (QWC) and general commutativity (GC). QWC requires Pauli operators on the same qubit to commute, whereas GC requires commutation as a whole. Two Pauli strings commute under GC if their Pauli operators anticommute at an even number (including zero) of qubit positions. Thus, QWC is a subset of GC and is computationally simpler. Graph-based methods can be used to identify commuting groups under QWC or GC.^{24–26} Elements in k -RDM can be mapped to Pauli strings, allowing commuting groups to be identified via QWC or GC.

The classical shadow²⁷ method employs randomized measurements to approximate quantum states and compute expectation values of observables, enabling partial tomography. Zhao et al.²⁸ extended the classical shadow for fermionic k -RDMs estimation by introducing an ensemble of fermionic Gaussian unitaries. Classical shadow can also be combined with additional strategies, such as leveraging symmetry¹⁸ as well as the N-representability conditions²⁹ of k -RDM to further reduce computational complexity.

The cumulant expansion method can also reduce computational costs. It decomposes RDMs as follows:

$$\begin{aligned}
 {}^1D &= {}^1\Delta \\
 {}^2D &= {}^2\Delta + {}^1\Delta \wedge {}^1\Delta \\
 {}^3D &= {}^3\Delta + 3{}^2\Delta \wedge {}^1\Delta + {}^1\Delta \wedge {}^1\Delta \wedge {}^1\Delta
 \end{aligned}
 \tag{16}$$

where ${}^k\Delta$ is the k -order connected RDM and \wedge represents the wedge product. It approximates k -RDMs by neglecting higher-order connected RDMs and summing lower-order terms. For example, if 1-RDM and 2-RDM are available, 3-RDM can be estimated as:

$${}^3D = 3^2\Delta \wedge^1 \Delta + {}^1\Delta \wedge^1 \Delta \wedge^1 \Delta \quad (17)$$

This method is particularly advantageous when the number of samples is limited or measurement errors are significant.³⁰

4 Error mitigation

Noise from quantum computers and measurement errors affect the accuracy of k -RDMs. Several methods have been developed to mitigate these errors.

4.1 Symmetry verification

The Hamiltonian \hat{H} in the active space commutes with the symmetry operator \hat{S} :

$$\hat{H}\hat{S} = \hat{S}\hat{H} \quad (18)$$

As a result, the ground and excited states must reside in one of the eigenspaces of \hat{S} (i.e., $\hat{S} = s$). However, during quantum computation, noise may cause the eigenstates of \hat{H} to deviate from their target eigenspace. Symmetry verification³¹ mitigates noise by using measurements during computation or post-selection to ensure that the ground or excited states remain within the desired subspace with projector $\hat{M}_s = \frac{1}{2}(1 + s\hat{S})$. The expectation

value of \hat{P} corresponding to the state ρ_s after symmetry verification is:

$$\begin{aligned}\mathrm{Tr}(\hat{P}\rho_s) &= \mathrm{Tr} \left[\hat{P} \frac{\hat{M}_s \rho \hat{M}_s}{\mathrm{Tr}(\hat{M}_s \rho)} \right] \\ &= \frac{\mathrm{Tr}(\hat{P}\rho) + s\mathrm{Tr}(\hat{P}\hat{S}\rho)}{1 + s\mathrm{Tr}(\hat{S}\rho)}\end{aligned}\tag{19}$$

This error mitigation process is computationally inexpensive.

4.2 N -representability conditions

The N -representability conditions impose constraints to ensure that a reconstructed k -RDM corresponds to a physically valid N -particle system.^{32–35}

In particular, the one-particle and one-hole RDMs are defined as

$${}^1D_q^p = \mathrm{Tr}[\hat{a}_p^\dagger \hat{a}_q, {}^N D], \quad {}^1Q_q^p = \mathrm{Tr}[\hat{a}_p \hat{a}_q^\dagger, {}^N D]\tag{20}$$

Ensuring their positive semidefiniteness,

$${}^1D \succeq 0, \quad {}^1Q \succeq 0\tag{21}$$

is both necessary and sufficient for N -representability in systems with only one-particle interactions. For two-particle correlations, we define the two-particle, two-hole, and particle-hole RDMs:

$$\begin{aligned}{}^2D_{rs}^{pq} &= \mathrm{Tr}[\hat{a}_p^\dagger \hat{a}_q^\dagger \hat{a}_s \hat{a}_r, {}^N D] \\ {}^2Q_{rs}^{pq} &= \mathrm{Tr}[\hat{a}_p \hat{a}_q \hat{a}_s^\dagger \hat{a}_r^\dagger, {}^N D] \\ {}^2G_{rs}^{pq} &= \mathrm{Tr}[\hat{a}_p^\dagger \hat{a}_q \hat{a}_s^\dagger \hat{a}_r, {}^N D]\end{aligned}\tag{22}$$

Two-positivity conditions require:

$${}^2D \succeq 0, \quad {}^2Q \succeq 0, \quad {}^2G \succeq 0 \quad (23)$$

There are relations between ${}^2D, {}^2Q$ and 2G :

$$\begin{aligned} {}^2Q_{k,l}^{i,j} &= 2 {}^2I_{k,l}^{i,j} - 4 {}^1D_k^i \wedge {}^1I_l^j + {}^2D_{k,l}^{i,j} \\ {}^2G_{k,l}^{i,j} &= {}^1I_l^j {}^1D_k^i - {}^2D_{k,j}^{i,l} \end{aligned} \quad (24)$$

1D and 1Q can be obtained from 2D and 2Q by contraction:

$${}^1D_k^i = \frac{1}{N-1} \sum_i {}^2D_{k,j}^{i,j}, \quad {}^1Q_k^i = \frac{1}{r-N-1} \sum_j {}^2Q_{k,j}^{i,j} \quad (25)$$

where r is the rank of the one-particle basis set. Similarly, there are multiple N-representation conditions for any k -RDMs. Note that k -positive conditions implies q -positive conditions for $k > q$. To reconstruct the k -RDM, we use the following semidefinite programming approach:³⁶

$$\begin{aligned} \min \quad & E(x) = c^T x \\ \text{s.t.} \quad & Ax = b, \quad M(x) \succeq 0. \end{aligned} \quad (26)$$

where the column vector c encodes the one- and two-electron integrals of the Hamiltonian and x is a column vector containing elements from all RDMs. The equation $Ax = b$ represents linear constraints on these RDMs. The block-diagonal matrix $M(x) \succeq 0$ ensures that the positivity conditions hold.

5 Simulation results

The RDM measurement-based PT-VQE method is employed to calculate the PESs of HF and N₂, as well as the ground-state energy of ferrocene (Fe(C₅H₅)₂). These computations

are performed with the quantum computational chemistry software Q²Chemistry.³⁷ The Jordan-Wigner (JW) transformation^{38,39} is used for fermion-to-qubit mapping.

5.1 Potential energy surfaces of small molecules

For HF and N₂, using the STO-3G basis, the full orbital spaces (HF:10e, 6o; N₂: 14e, 10o) are divided into an inactive space consisting of the three lowest-energy molecular orbitals (6e, 3o) and an active space comprising the remaining orbitals (HF: 4e, 3o; N₂: 8e, 7o). Excluding excitations that act only within the active space reduces the highest measured RDM in PT-VQE from 4-RDM to 3-RDM. As shown in Fig. 2, for both HF and N₂, PT-VQE with the highest 4-RDM and 3-RDM produce identical energies at all bond lengths. These energies achieve chemical accuracy at most bond lengths for N₂ and all bond lengths for HF, with significantly smaller errors than VQE.

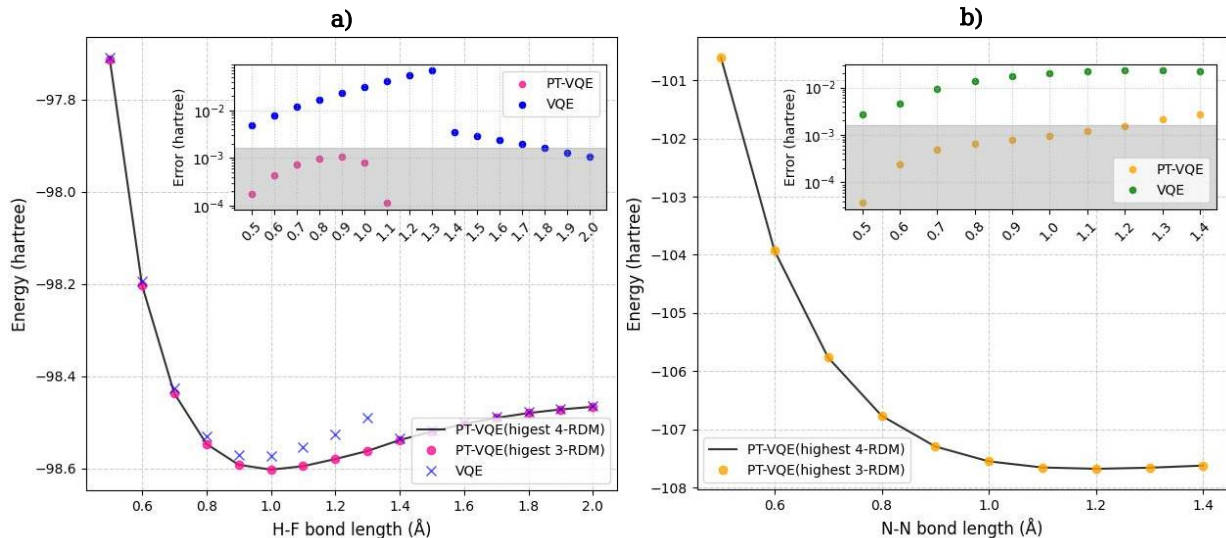


Figure 2 PESs for (a) HF and (b) N₂ calculated using PT-VQE with the highest-order RDM as 4-RDM and 3-RDM, respectively. Insets show the errors for PT-VQE and VQE, with the shaded region indicating chemical accuracy.

5.2 Ground-state energy of ferrocene

The geometry of ferrocene ($\text{Fe}(\text{C}_5\text{H}_5)_2$) consists of two cyclopentadienyl (Cp) rings parallel to the z-axis, with an iron atom sandwiched between them, as shown in Fig. 3. The ground state is primarily determined by the Fe d orbitals and the Cp π orbitals. Using the atomic valence active space⁴⁰ technique, we first select atomic orbitals associated with Fe $3d$ orbitals, forming a (10e, 7o) active space, as also described in Ref. 40. In this space, the VQE solution corresponds to the Hartree-Fock state. The energy obtained using VQE is -1655.96073 hartree. Then we include the $2p_z$ orbitals of C to construct an (8e, 8o) perturbative space. The PT-VQE method is used in a (18e, 15o) space combined with active and perturbative spaces. After perturbation, the ground-state energy is -1655.96129 hartree, with an error of 4.097×10^{-5} hartree, compared to the complete active space configuration interaction (CASCI) energy of -1655.96133 hartree. If we reduce those excitations that excites only inside the active space, the energy after perturbation is still -1655.96129 hartree.

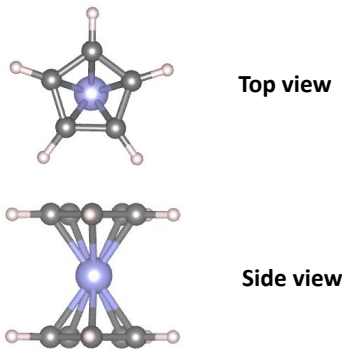


Figure 3 Geometry of ferrocene

6 Hardware calculation of F_2 ground-state energy

We apply PT-VQE method to compute the ground-state energy of F_2 on a real quantum computer. The experiment was performed on the Baihua chip, part of the five-hundred-qubit cluster in the Quafu quantum cloud platform.⁴¹ Further details are provided in the

Supporting Information.

In the STO-6G basis, the active space includes the 3 A_{1u} and 3 A_{1g} molecular orbitals in $D_{\infty h}$ symmetry, which capture the key bonding and anti-bonding interactions of the F-F bond. The lowest two molecular orbitals are frozen, as shown in Fig. 4 (b). For this 4-qubit active space, the following ansatz $\hat{U}(\theta)$ is used in VQE method:

$$\hat{U}(\theta) = e^{-i\frac{\theta}{2}X_0X_1X_2Y_3} \quad (27)$$

Applied to the initial state $|1100\rangle$, it produce $|1100\rangle$ and $|0011\rangle$ configurations. The corresponding circuit is shown in Fig. 4 (c). To reduce experimental errors, the circuit is simplified to Fig. 4 (d). Both circuits are equivalent, but the simplified one uses fewer two-qubit gates. The initial state in the simplified circuit is $|1000\rangle$.

The ground reference state $|\Psi_0\rangle = |\Psi_{\text{inact}}\rangle \otimes |\Psi_{\text{act}}\rangle$, where $|\Psi_{\text{inact}}\rangle$ is the state with all perturbative orbitals doubly occupied. Excitations $\{\hat{r}_2^{uv}, \hat{r}_{u1}^{v\bar{v}}, \hat{r}_{1\bar{1}}^{v\bar{v}}, \hat{r}_{2\bar{2}}^{v\bar{v}}, \hat{r}_{3\bar{3}}^{v\bar{v}}, \hat{r}_{4\bar{4}}^{v\bar{v}}, \hat{r}_{5\bar{5}}^{v\bar{v}}, \hat{r}_{6\bar{6}}^{v\bar{v}}, \hat{r}_{u\bar{u}}^{v\bar{v}}\}$ are selected to promote electrons from the doubly occupied perturbative space to the active space. The ground-state energy after perturbation is obtained only using the VQE circuit, as discussed in Section 2.

All experimental data are Bayesian-corrected. The Hamiltonian in the active space commutes with the symmetry operator $\hat{S} = Z_0Z_1Z_2Z_3$, and the ground state belongs to the subspace where $\hat{S} = 1$. According to Eq. (19), the expectation values of \hat{P} and $\hat{P}\hat{S}$ are equivalent. Thus, we use symmetry verification as a post-selection method to filter out noisy measurements. Furthermore, since the circuit prepares a two-electron system fully described by the 2-RDM, we mitigate unphysical artifacts caused by errors by enforcing N -representability conditions.

Fig. 5 illustrates the calculated ground-state energies and corresponding errors for F_2 at different bond lengths using VQE and PT-VQE, with and without symmetry verification (SV) and RDM reconstruction based on N -representability conditions. PT-VQE consistently

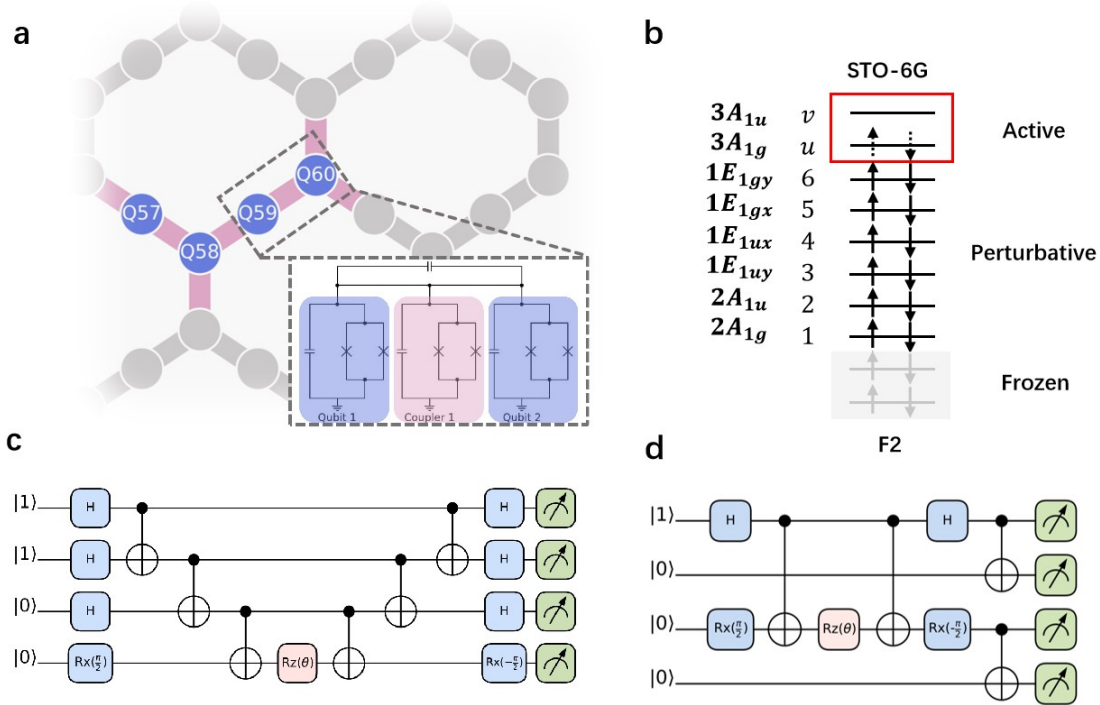


Figure 4 (a) Chip structure featuring a hexagonal qubit arrangement with adjustable couplers. (b) Spatial partitioning and orbital symmetry of F₂ (c) Original ansatz circuit. (d) Simplified circuit.

outperforms standard VQE, significantly reducing errors. As shown in the upper panel, the average errors for PT-VQE are 0.0238 (raw), 0.0075 (SV), and -0.0012 (SV+RDM) hartree, notably lower than those for standard VQE: 0.0898 (raw), 0.0149 (SV), and 0.0059 (SV+RDM) hartree. With both SV and RDM reconstruction, PT-VQE achieves chemical accuracy across most bond lengths.

7 Conclusion

To bridge the gap between the resource demands of practical applications and the limitations of current NISQ devices, we propose the PT-VQE method. PT-VQE combines VQE with perturbation theory to efficiently approximate ground-state energy. VQE constructs a reference ground state within the active space, while perturbation corrections account for contributions from the perturbative space, refining the accuracy of the ground state and its

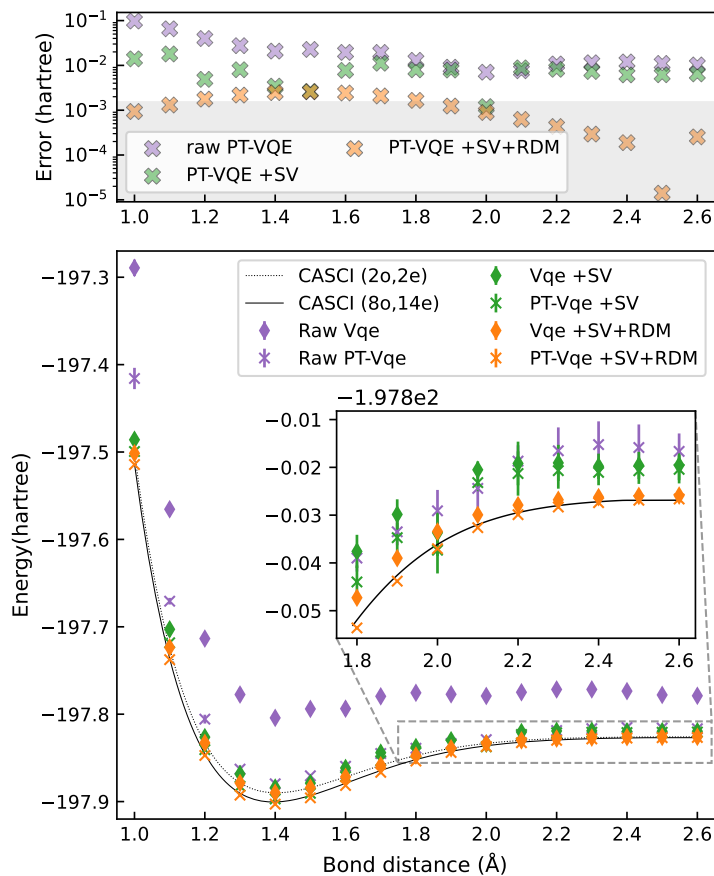


Figure 5 Lower panel: Ground-state PESs of F_2 calculated using CASCI and VQE within a 2-orbital, 2-electron active space, and CASCI and PT-VQE within a larger 8-orbital, 14-electron active space. Results are shown for raw data, data processed with symmetry verification (SV), as well as SV combined with RDM reconstruction. Upper panel: Absolute errors in the PT-VQE results, with the shaded region indicating values within chemical accuracy.

energy.

A key advantage of PT-VQE is its reduced computational cost. Instead of measuring the full wavefunction, it requires only up to 4-RDM. Furthermore, if the VQE-optimized state closely approximates the true ground state in the active space, excitations cannot act solely within the active space, as their perturbative contributions are negligible. This further lowers the highest required RDM to 3-RDM.

We validate PT-VQE by simulating the ground-state PESs of HF and N_2 and the ground-state energy of ferrocene ($Fe(C_5H_5)_2$), using both 4-RDM and 3-RDM constraints. The results are consistent, confirming the validity of restricting excitations. Additionally, we

compute the PES of F_2 molecule on the Quafu superconducting quantum computer. Without increasing qubit count or circuit depth, PT-VQE achieves several-fold higher precision than standard VQE, reaching chemical accuracy at most bond lengths.

With its reduced computational cost, PT-VQE enables significant quantum chemistry calculations even in the NISQ era.

8 Acknowledgments

This work was supported by Innovation Program for Quantum Science and Technology (2021ZD0303306), the National Natural Science Foundation of China (22073086, 22393913).

9 Conflicts of interest

There are no conflicts of interest to declare.

References

- (1) Szalay, P. G.; Müller, T.; Gidofalvi, G.; Lischka, H.; Shepard, R. Multiconfiguration Self-Consistent Field and Multireference Configuration Interaction Methods and Applications. *Chem. Rev.* **2012**, *112*, 108–181.
- (2) Holmes, A. A.; Tubman, N. M.; Umrigar, C. J. Heat-Bath Configuration Interaction: An Efficient Selected Configuration Interaction Algorithm Inspired by Heat-Bath Sampling. *J. Chem. Theory Comput.* **2016**, *12*, 3674.
- (3) Liu, W.; Hoffmann, M. R. iCI: Iterative CI toward full CI. *J. Chem. Theory Comput.* **2016**, *12*, 1169.
- (4) Levine, D. S.; Hait, D.; Tubman, N. M.; Lehtola, S.; Whaley, K. B.; Head-Gordon, M.

- CASSCF with Extremely Large Active Spaces Using the Adaptive Sampling Configuration Interaction Method. *J. Chem. Theory Comput.* **2020**, *16*, 2340–2354.
- (5) Tubman, N. M.; Freeman, C. D.; Levine, D. S.; Hait, D.; Head-Gordon, M.; Whaley, K. B. Modern Approaches to Exact Diagonalization and Selected Configuration Interaction with the Adaptive Sampling CI Method. *J. Chem. Theory Comput.* **2020**, *16*, 2139.
- (6) Booth, G. H.; Thom, A. J. W.; Alavi, A. Fermion Monte Carlo Without Fixed Nodes: A Game of Life, Death, and Annihilation in Slater Determinant Space. *J. Chem. Phys.* **2009**, *131*, 054106.
- (7) Cleland, D.; Booth, G. H.; Alavi, A. Communications: Survival of the Fittest: Accelerating Convergence in Full Configuration-Interaction Quantum Monte Carlo. *J. Chem. Phys.* **2010**, *132*, 041103.
- (8) White, S. R. Density Matrix Formulation for Quantum Renormalization Groups. *Phys. Rev. Lett.* **1992**, *69*, 2863.
- (9) Chan, G. K.-L.; Sharma, S. The Density Matrix Renormalization Group in Quantum Chemistry. *Annu. Rev. Phys. Chem.* **2011**, *62*, 465.
- (10) Eriksen, J. J.; Lipparini, F.; Gauss, J. Virtual Orbital Many-Body Expansions: A Possible Route towards the Full Configuration Interaction Limit. *J. Phys. Chem. Lett.* **2017**, *8*, 4633.
- (11) Eriksen, J. J.; Gauss, J. Generalized Many-Body Expanded Full Configuration Interaction Theory. *J. Phys. Chem. Lett.* **2019**, *10*, 7910.
- (12) Pulay, P. A perspective on the CASPT2 method. *Int. J. Quantum Chem.* **2011**, *111*, 3273–3279.

- (13) Angeli, C.; Cimiraglia, R.; Evangelisti, S.; Leininger, T.; Malrieu, J.-P. Introduction of n-electron valence states for multireference perturbation theory. *J. Chem. Phys.* **2001**, *114*, 10252–10264.
- (14) Ryabinkin, I. G.; Izmaylov, A. F.; Genin, S. N. A posteriori corrections to the iterative qubit coupled cluster method to minimize the use of quantum resources in large-scale calculations. *Quantum Sci. Technol.* **2021**, *6*, 024012.
- (15) Liu, J.; Li, Z.; Yang, J. Perturbative variational quantum algorithms for material simulations. *Electron. Struct.* **2024**, *6*, 015007.
- (16) Tamaro, A.; Galli, D. E.; Rice, J. E.; Motta, M. N-Electron Valence Perturbation Theory with Reference Wave Functions from Quantum Computing: Application to the Relative Stability of Hydroxide Anion and Hydroxyl Radical. *jpca* **2023**, *127*, 817–827.
- (17) Liepuoniute, I.; Motta, M.; Pellegrini, T.; Rice, J. E.; Gujarati, T. P.; Gil, S.; Jones, G. O. Simulation of a Diels-Alder reaction on a quantum computer. *Phys. Chem. Chem. Phys.* **2024**, *26*, 25181–25191.
- (18) Smart, S. E.; Mazziotti, D. A. Lowering tomography costs in quantum simulation with a symmetry projected operator basis. *Phys. Rev. A* **2021**, *103*, 012420.
- (19) Grimsley, H. R.; Economou, S. E.; Barnes, E.; Mayhall, N. J. An adaptive variational algorithm for exact molecular simulations on a quantum computer. *Nat. Commun.* **2019**, *10*, 1–9.
- (20) Helgaker, T.; Jorgensen, P.; Olsen, J. *Molecular electronic-structure theory*, 1st ed.; John Wiley & Sons: Chichester, UK, 2013; pp 710–713.
- (21) Chan, H. H. S.; Fitzpatrick, N.; Segarra-Martí, J.; Bearpark, M. J.; Tew, D. P. Molecular excited state calculations with adaptive wavefunctions on a quantum eigensolver

- emulation: reducing circuit depth and separating spin states. *Phys. Chem. Chem. Phys.* **2021**, *23*, 26438–26450.
- (22) Sakurai, J. J.; Napolitano, J. In *Modern Quantum Mechanics*, 2nd ed.; Kenney, L., Conley, K., Benson, C., Eds.; Jim Smith: Cambridge University, U.S., 2020; pp 309–310.
- (23) Zheng, Y.; Sun, Z.; Liu, J.; Fan, Y.; Li, Z.; Yang, J. Quantum Equation-of-Motion Method with Single, Double, and Triple Excitations. *J. Chem. Theory Comput.* **2024**, *20*, 9032–9040.
- (24) Tilly, J.; Chen, H.; Cao, S.; Picozzi, D.; Setia, K.; Li, Y.; Grant, E.; Wossnig, L.; Rungger, I.; Booth, G. H.; others The variational quantum eigensolver: a review of methods and best practices. *Phys. Rep.* **2022**, *986*, 1–128.
- (25) Verteletskyi, V.; Yen, T.-C.; Izmaylov, A. F. Measurement optimization in the variational quantum eigensolver using a minimum clique cover. *J. Chem. Phys.* **2020**, *152*.
- (26) Gokhale, P.; Angiuli, O.; Ding, Y.; Gui, K.; Tomesh, T.; Suchara, M.; Martonosi, M.; Chong, F. T. Minimizing state preparations in variational quantum eigensolver by partitioning into commuting families. *arXiv preprint arXiv:1907.13623* **2019**,
- (27) Huang, H.-Y.; Kueng, R.; Preskill, J. Predicting many properties of a quantum system from very few measurements. *Nat. Phys* **2020**, *16*, 1050–1057.
- (28) Zhao, A.; Rubin, N. C.; Miyake, A. Fermionic partial tomography via classical shadows. *Phys. Rev. Lett.* **2021**, *127*, 110504.
- (29) Avdic, I.; Mazziotti, D. A. Fewer Measurements from Shadow Tomography with N-Representability Conditions. *Phys. Rev. Lett.* **2024**, *132*, 220802.
- (30) Takemori, N.; Teranishi, Y.; Mizukami, W.; Yoshioka, N. Balancing error budget for fermionic k-RDM estimation. *arXiv preprint arXiv:2312.17452* **2023**,

- (31) Bonet-Monroig, X.; Sagastizabal, R.; Singh, M.; O’Brien, T. E. Low-cost error mitigation by symmetry verification. *Phys. Rev. A* **2018**, *98*, 062339.
- (32) Coleman, A. J.; Rosina, M.; Mazziotti, D. A.; Erdahl, R. M.; Braams, B. J.; Percus, J. K.; Zhao, Z.; Fukuda, M.; Nakata, M.; Yamashita, M.; others In *Reduced-density-matrix mechanics: with application to many-electron atoms and molecules*; David A. Mazziotti, S. A. R., Ed.; John Wiley & Sons: Hoboken, New Jersey, 2007; Vol. 134; pp 21–48.
- (33) Rubin, N. C.; Babbush, R.; McClean, J. Application of fermionic marginal constraints to hybrid quantum algorithms. *New J. Phys.* **2018**, *20*, 053020.
- (34) Cai, Z.; Babbush, R.; Benjamin, S. C.; Endo, S.; Huggins, W. J.; Li, Y.; McClean, J. R.; O’Brien, T. E. Quantum error mitigation. *Rev. Mod. Phys.* **2023**, *95*, 045005.
- (35) Smart, S. E.; Mazziotti, D. A. Quantum-classical hybrid algorithm using an error-mitigating N-representability condition to compute the Mott metal-insulator transition. *Phys. Rev. A* **2019**, *100*, 022517.
- (36) Mazziotti, D. A. Large-scale semidefinite programming for many-electron quantum mechanics. *Phys. Rev. Lett.* **2011**, *106*, 083001.
- (37) Fan, Y.; Liu, J.; Zeng, X.; Xu, Z.; Shang, H.; Li, Z.; Yang, J. Q²Chemistry: A quantum computation platform for quantum chemistry. *arXiv preprint arXiv:2208.10978* **2022**,
- (38) Jordan, P.; Wigner, E. Über das Paulische Äquivalenzverbot. *Eur. Phys. J. A* **1928**, *47*, 631–651.
- (39) Fradkin, E. Jordan-Wigner transformation for quantum-spin systems in two dimensions and fractional statistics. *Phys. Rev. Lett.* **1989**, *63*, 322.
- (40) Sayfutyarova, E. R.; Sun, Q.; Chan, G. K.-L.; Knizia, G. Automated construction of

molecular active spaces from atomic valence orbitals. *J. Chem. Theory Comput.* **2017**, *13*, 4063–4078.

(41) Q. Quafu website. <https://quafu.baqis.ac.cn/> (2024).

Appendices

1. Device information

The experiment was conducted on the Baihua chip, part of the 500-qubit cluster on the Quafu quantum cloud platform. Baihua is a superconducting quantum processor with 156 quantum qubits and 172 tunable couplers. Each qubit is connected to 2 or 3 adjacent couplers, except for those at the edge of the lattice. We use 4 qubits in them: Q57, Q58, Q59, Q60. The basic parameters and gate fidelity of these four qubits are shown in Table 1.

Table 1 Basic parameters and gate fidelity of qubits

	Q57	Q58	Q59	Q60
Qubit frequency(GHz)	4.066	4.407	4.134	4.396
Anharmonicity(GHz)	0.196	0.178	0.193	0.181
Readout frequency(GHz)	6.754	7.063	6.799	7.109
T1(us)	63.9	63.9	82.7	62.4
T2 Ramsey(us)	35.8	21.4	19.6	28.3
single-qubit gate fidelity(%)	99.93	99.93	99.94	99.93
CZ gate fidelity(%)		98.5	99.2	98.7